Journal of
Marine Science and Engineering

MDPI

Article

Study on Complex Wake Characteristics of Yawed Wind Turbine Using Actuator Line Method

Tengyuan Wang [1,2], Shuni Zhou [3,4], Chang Cai [1,*], Xinbao Wang [1,5], Zekun Wang [1,2], Yuning Zhang [2], Kezhong Shi [1], Xiaohui Zhong [1] and Qingan Li [1,5,*]

1 CAS Laboratory of Wind Energy Utilization, Institute of Engineering Thermophysics, Chinese Academy of Sciences, Beijing 100190, China
2 School of Energy, Power and Mechanical Engineering, North China Electric Power University, Beijing 102206, China
3 Guangdong Haizhuang Offshore Windpower Research Center Company Limited, Zhanjiang 524100, China
4 Southern Marine Science and Engineering Guangdong Laboratory (Zhanjiang), Zhanjiang 524013, China
5 University of Chinese Academy of Sciences, Beijing 100049, China
* Correspondence: caichang@iet.cn (C.C.); liqingan@iet.cn (Q.L.)

Abstract: In modern large-scale wind farms, power loss caused by the wake effect is more than 30%, and active yaw control can greatly reduce the influence of the wake effect by deflecting the wind turbine's wake. The yawed wind turbine's wake characteristics are complex, and a deep comprehension of a yawed turbine's wake is necessary. The actuator line method combined with URANS (unsteady Reynold-averaged Navier–Stokes equations) is used to study the yawed wind turbine's wake characteristics in this paper. Compared with an un-yawed wind turbine, a yawed one has two main characteristics, deflection and deformation. With an increasing yaw angle, turbine wake shows an increasing deflection. The results indicated that deflection at different height was different, the wake profile showed the biggest deflection at about the hub height, while the smallest deflection existed at the top and bottom of the yawed turbine's wake. This can be visually demonstrated by the evolution of a kidney-shape velocity distribution at the vertical cross-section. Two-dimensional and three-dimensional presentations of velocity deficit distributions are presented in this paper. The evolution of an irregular kidney-shape distribution is discussed in this paper. It is formed by the momentum exchange caused by the counter-rotating vortex pair. The results indicated that the counter-rotating vortex pair was composed of the streamwise vortex flux brought by the tip vortex. Furthermore, when the wind turbine rotated clockwise and yawed clockwise, the negative vorticity of counter-rotating vortex first appeared in the upper left position.

Keywords: wind turbine; wake effect; yaw condition; actuator line method

check for updates

Citation: Wang, T.; Zhou, S.; Cai, C.; Wang, X.; Wang, Z.; Zhang, Y.; Shi, K.; Zhong, X.; Li, Q. Study on Complex Wake Characteristics of Yawed Wind Turbine Using Actuator Line Method. *J. Mar. Sci. Eng.* **2023**, *11*, 1039. https://doi.org/10.3390/jmse11051039

Academic Editor: Unai Fernandez-Gamiz

Received: 18 April 2023
Revised: 27 April 2023
Accepted: 9 May 2023
Published: 12 May 2023

1. Introduction

With the growing number of large modern wind farms, the transition to net zero has been accelerated by the speedy development of wind power. The negative impact of the wake effect is non-negligible. The literature shows that the downstream wind turbine's power loss is over 30% [1–3]. Free stream blows into the turbine rotor, the wind turbine rotor absorbs the wind energy and powers the generator. In the downstream flow field of a wind turbine, a velocity deficit is generated that decreases the downstream wind turbine's power generation [4,5].

Wind turbines are generally conceptually divided into the near wake and the far wake [6,7]. In the near wake, a bimodal distribution with a double Gaussian shape is representative of the turbine's wake profile. This can be understood from the perspective of energy conversion: The hub of the wind turbine does not have the ability to absorb wind energy, so wind speed is higher in the middle part of turbine wake, resulting in a bimodal distribution. With continuous mixing of external turbulence flow, the wake expands gradually and develops a unimodal Gaussian distribution wake profile in the far wake. A vortex structure plays an important role in wake development and evolution: Velocity circulation around the blade element is the root cause of lift force. It falls off the blade tip and is transported into the near wake; the velocity-induced effect of the vortex component of the tip vortex on a parallel wind rotor can be described by the Biot–Savart Law [8]. The tip vortex falls off from the wind turbine in a spiral trajectory, and a leapfrogging behavior occurs in the near wake area [9] that enhances the instability and recovery of the turbine's wake. It should be noted that the strength and shedding mode of a tip vortex are closely related to the wind turbine's parameters and operating conditions. Besides the wind turbine aspect, atmospheric stability and turbulence intensity are also important factors affecting wake development and evolution [10]; the wake recovery rate is slower in a stable atmosphere.

Various methods have been adopted by researchers to study turbines' wake [11]. Wake measurements of small-scale wind turbines in a wind tunnel [12–14] is an effective way to obtain experimental data. Thrust coefficient, power coefficient and tip ratio are important factors to be considered in the design of a wind turbine model. Experimental instruments such as a hot-wire anemometer, laser Doppler velocimetry (LDV) and particle image velocimetry (PIV) are widely adopted in the wake measurement under controlled conditions. Cheng et al. [15] conducted a wind tunnel experiment to explore the interaction between the turbine wake and the boundary flow over a forest. Field measurements are also indispensable. In recent years, wind mast, SODAR (Sonic Detection and Ranging) and LiDAR (Light Detection and Ranging) [16,17] have been adopted in wake measurements of wind farms. Compared with wind tunnel measurements, field measurements are uncontrollable, which means that field measurements generally require a longer measurement period and have higher economic costs. Different numerical simulation methods have been adopted in studies of turbine wake [18–20]. The actuator model is the most widely used approach because of low computational cost and high accuracy. It is also noted that a computational fluid dynamics (CFD) simulation of a wind farm's wake effect basically adopts the actuator model method. These data acquisition methods have their own advantages and disadvantages and are suitable for different situations.

To evaluate the wake effect on a wind farm's power generation, so as to optimize layout and develop a control strategy, researchers have been studying an engineering wake model for decades. The Jensen model [21] is a simple one-dimensional analytical wake model and is widely used; a uniform velocity deficit with a top-hat shape is adopted in this model. A classical Gaussian wake model was proposed by Bastankhah and Porté-Agel [22] that predicts the velocity distribution more accurately. Generally, the engineering wake model consists of three parts. The first part is the wake turbulence intensity model. It is generally believed that the turbulence intensity of wake determines the rate of wake expansion. The turbulence intensity is determined by the ambient turbulence intensity and the turbulence intensity added by the wind turbine. The latter is related to the thrust coefficient of the wind turbine. The second part is the wake expansion model that is mainly related to turbulence intensity. Du et al. [23] recently proposed a wake expansion model considering atmospheric stability. In the third part, mass conservation and momentum conservation are used to obtain the total velocity deficit. Then, the velocity deficit is redistributed with a Gaussian shape. A cosine shape has been used by Tian et al. [24] and accords well with field measurements.

Reducing the impact of the wake effect on power generation has always been the focus of researchers [25]. In order to gain more windward area, a wind turbine is programmed to keep track of the wind direction by adjusting the azimuth. Under the influence of such a greedy control strategy, the wake effect's impact on a downstream wind turbine's performance is enhanced and results in a considerable power loss [26–28]. Expanding the space between wind turbines is the most straightforward approach to reducing the impact of the wake effect; however, construction and operating costs limit the layouts of wind farms. In recent years, wind farm cooperative control has been regarded as an effective way to reduce wake effects, and active yaw control (AYC) is a prominent control strategy [29]. When an upstream wind turbine is yawed, the turbine's wake can be deflected by a transverse component of the axial thrust, which decreases the wake effect's influence on a downstream wind turbine's performance. Although upstream wind turbine's power generation decreases due to yaw control, the increase of downstream wind turbine's power generation enhances the overall performance. According to wind tunnel measurements conducted by Zong and Porté-Agel [14], a power increase of 18% can be achieved by yawing wind turbines in a miniature wind farm. Yang et al. [30] proposed a new machine learning method for cooperative yaw control in a wind farm, and a notable power improvement could be obtained. Tilt or yaw angles of an upstream wind turbine have been changed by Nakhchi et al. [31]; simulations indicated that the total power performance of tandem wind turbines could be increased by 6.1%. These studies indicate that yaw control can significantly enhance the power performance in a tandem wind turbines small-scale cluster.

Reasonable active yaw control can also significantly enhance the power performance of a modern large wind farm. Based on a proposed analytical engineering wake model, Dou et al. [32] optimized the yaw angle of each wind turbine to enhance the total power performance, resulting in a power increase of 18%. Considering active yaw control, Song et al. [33] developed a particle-swarm-optimization-based method for wind farm layout optimization. The results showed that the total power generation was enhanced by 4.32%. Ma et al. [34] optimized yaw angles of each wind turbine to enhance the overall power performance. The results showed that the power increase reached 17.5%. Active yaw control was applied in an offshore wind farm with an optimized layout by Li et al. [35]. The results showed that the total power increased by 2.1%. It can be seen that a power increase of 2–18% can be obtained with different wind farm and active yaw control strategies.

A deep understanding of wake characteristics in yaw conditions is the basis of active yaw control. Dou et al. [36] conducted a typical wind tunnel measurement and proposed an analytical wake model for a yawed turbine. The deflection of wake was described by a semi-empirical formula. Zhu et al. [37] conducted a field wake measurement using LiDAR and established a three-dimensional non-uniform wake model. Its results show that the model agrees well with experimental data. Jiménez et al. [38] conducted a large eddy simulation (LES) of a yawed wind turbine's wake, and wake deflection was evaluated. Numerous studies have shown the complexity of the wind turbine's wake in yaw conditions. The projection surface of a yawed turbine in the direction of incoming wind is of elliptical shape, which is a symmetrical distribution. However, many studies have shown that the turbine wake in yaw conditions is significantly asymmetrical. Micallef et al. [39] believe that the complex flow in the blade tip and blade root is responsible for the complex wake characteristics in yaw conditions. Howland et al. [40] conducted an LES simulation with both an actuator disk model (ADM) and an actuator line model (ALM). Their study shows that a symmetrical kidney-shape velocity deficit appears in the vertical cross-section of ADM simulation results, while an asymmetrical kidney-shape velocity deficit appears in the vertical cross-section of ALM simulation results. Bastankhah and Porté-Agel [13] conducted a representative wind tunnel experiment with PIV. They believe that the existence of a counter-rotating vortex pair is responsible for the complex deformation of a yawed turbine's wake. Furthermore, a qualitative analysis of a counter-rotating vortex pair based on measured data and a continuity equation is presented in their study. Based on the lift line theory, Shapiro et al. [41] proposed a symmetrical theoretical counter-rotating vortex pair model. In their theoretical model, the two counter-rotating vortexes have the same strength. Recently, a new proposed generation mechanism of a counter-rotating vortex pair has been presented by Wang et al. [42]. Their study shows that the streamwise vorticity carried by the blade tip vortex is the reason for the generation of counter-rotating vortex pairs. Based on that, an asymmetrical theoretical counter-rotating vortex pair model has been proposed. In summary, the complex wake characteristics of a yawed wind turbine need further investigation.

A simulation using an actuator line method was adopted in this study. The actuator line method for studying a wind turbine's wake has been proposed by Sørensen and

Shen [18]. Two significant advantages make ALM stand out: it can accurately reproduce the vortex structure of a turbine's wake and simulate the turbine's wake flow field. Additionally, the computational cost is low since there is much less mesh. In Section 2, the numerical approaches are introduced; ALM was adopted to simulate the wind turbine. In Section 3, the wake characteristics of different section are presented and analyzed.

2. Numerical Approaches

An ALM-combined URANS simulation was adopted in this paper. Considering a different yaw angle, the turbine wake of an NREL 5-MW wind turbine was simulated.

2.1. Actuator Line Model

The force generated by the blades is replaced by the actuator point (shown in Figure 1), the force is distributed in the computation domain with the form of a force source term. The force source term is obtained by blade element theory [43] and is distributed in a Gaussian way. An ALM simulation is a relatively low-computational-cost approach for a turbine's wake simulation because the precise simulation of the flow field around the blade is abandoned.

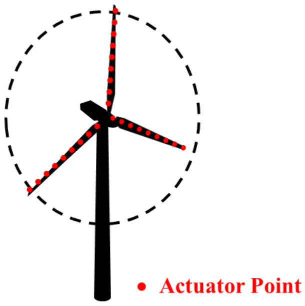

Figure 1. Schematic of ALM.

The velocity triangle of the blade element is shown in Figure 2. The resultant wind speed of the blade element consists of wind speed and blade rotation speed:

$$W = \sqrt{u_a^2 + (u_t - \omega r)^2}, \tag{1}$$

therefore, inflow angle φ can be obtained:

$$\varphi = \arcsin(u_a/w), \tag{2}$$

then, the attack angle α is:

$$\alpha = \varphi - \beta. \tag{3}$$

Based on lift and drag coefficient of airfoil characteristics:

$$f = (L, D) = \frac{1}{2}\rho W^2 c(C_L e_L + C_D e_D). \tag{4}$$

In order to avoid a concentrated distribution of source terms, a Gaussian distribution method was adopted:

$$f_\epsilon = f \otimes \eta_\epsilon, \tag{5}$$

$$\eta_\epsilon(r) = \frac{1}{\epsilon^3 \pi^{3/2}} \exp\left[-(d/\epsilon)^2\right]. \tag{6}$$

More details of the ALM simulation can be found in [18].

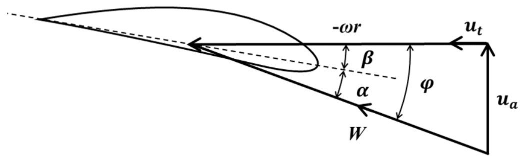

Figure 2. Velocity triangle of the blade element.

2.2. Simulation Settings and Validation

Wake of a NREL 5-MW wind turbine [44] was simulated in this paper. NREL 5–MW is a classic offshore wind turbine design by Jonkman et al. The rated power of this turbine is 5 MW, and the diameter of the wind turbine is 126 m. Since the design parameters of this wind turbine are detailed, the research object of many studies is the NREL 5–MW wind turbine.

The computational domain is shown is Figure 3. A sufficiently long inlet section and outlet section ensure the full development of aerodynamic performance of the wind turbine and turbine's wake. The fine mesh around the wind turbine ensures the accurate calculation of the aerodynamic characteristics of the wind turbine. Additionally, the k-ω SST turbulence model was adopted.

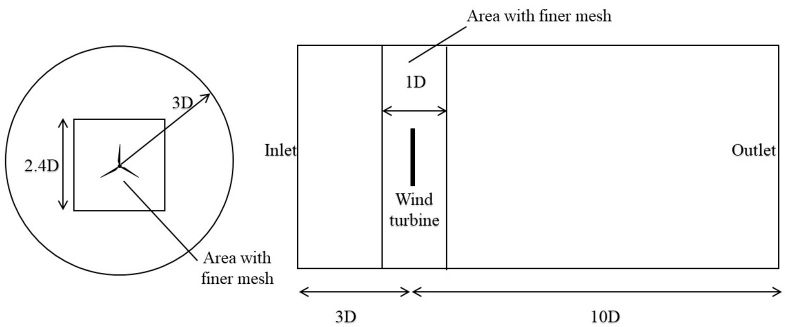

Figure 3. Computational domain.

Figure 4 shows the power coefficient under different tip speed ratios. It shows that the ALM calculation results predicted the overall power performance of the NREL 5-MW wind turbine. With the increase of the tip ratio, the power coefficient increased first and then decreased; the optimal tip ratio was 7.55.

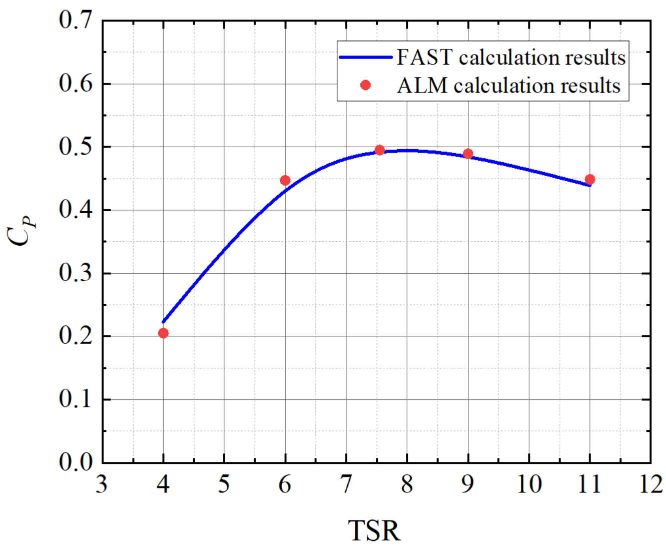

Figure 4. Power coefficient under different tip speed ratios.

3. Results and Discussion

In this section, the wake characteristics with yaw angles of 0°, 10°, 15°, 20°, 25° and 30° are analyzed and discussed. The TSR of the wind turbine was 7.55, and the incoming wind speed was 8 m/s.

3.1. Velocity Deficit at Different Horizontal Section

Figure 5 is the dimensionless wake velocity contours of a yawed turbine's wake, and wake profiles at three heights (R represents the rotor radius) of each yaw condition are shown. When the wind turbine is not in a yaw condition, the turbine's wake has a basically central symmetrical shape, which means that the wake velocity cross-sections 0.5 R above the hub height and 0.5 R below the hub height are basically the same.

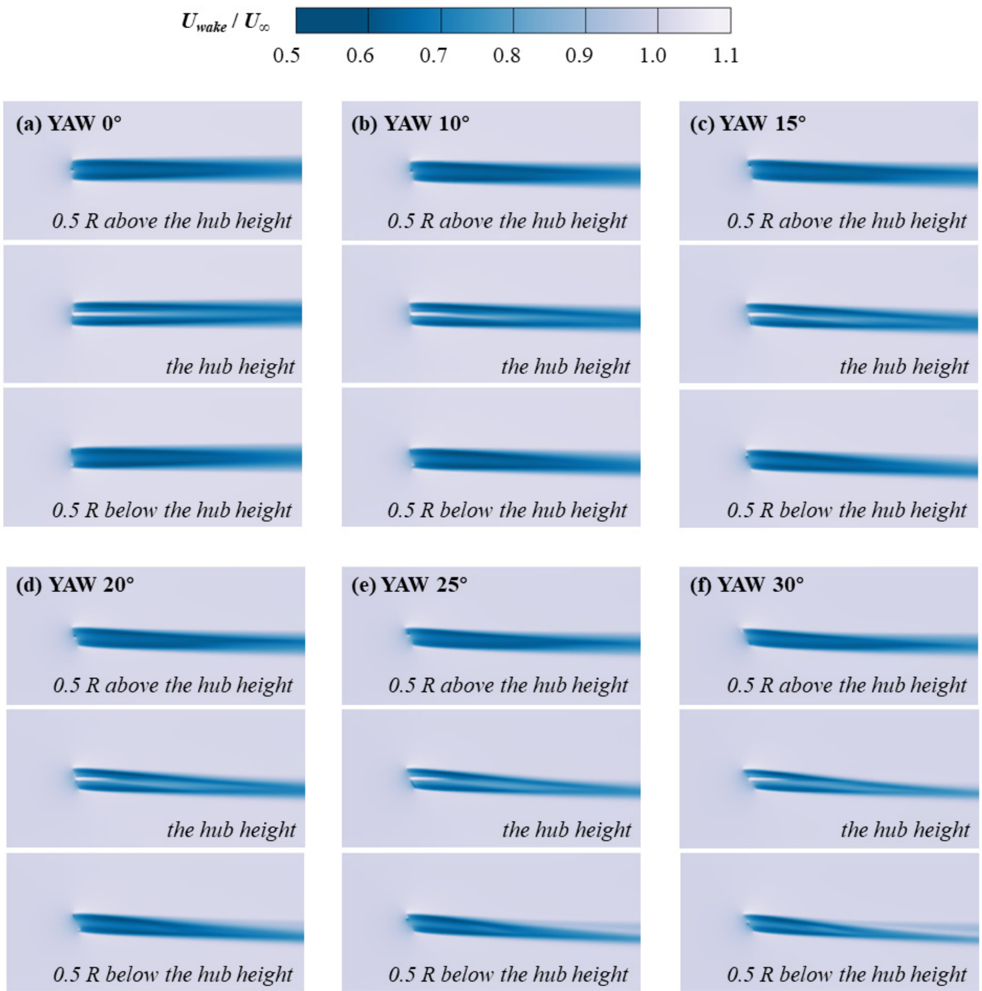

Figure 5. Dimensionless wake velocity contours at different heights.

A noticeable deflection could be observed when the wind turbine was in a yaw condition. The turbine's wake deflected to one side that was opposite to the yaw direction. This can be explained by the conservation of momentum in the lateral direction. The lateral component of the axial thrust of the wind turbine caused the deflection of the wake. With the yaw angle increasing, the deflection degree of the yawed turbine's wake increased; however, the increase of the wake deflection below the hub height was much more obvious. The inconsistency of the wake deflection degree at different altitudes is one of the important characteristics of a yawed turbine's wake. In addition to the degree of deflection, the wake shape of the yawed wind turbine varied at different height sections, and the central symmetry of wake velocity distribution of the un-yawed wind turbine was no longer applicable. It can be seen in Figure 5 that the wake profiles at 0.5 R above the hub height and 0.5 R below the hub height were not the same, and the wake width at the lower height section was smaller. Furthermore, the wake width of the far wake decreased with the increasing of yaw angle, which was much more obvious at hub height and 0.5 R below the hub height. Based on the above analysis, simple two-dimensional engineering wake analytical models may not be competent to describe the complex velocity deficit distribution of a yawed turbine's wake.

Figure 6 shows the yawed turbine's wake profiles with different yaw angles. The results showed that when the wind turbine was not in a yaw condition, the upper wake profile (0.5 R above the hub height) and lower wake profile (0.5 R below the hub height) were almost overlapping. When the wind turbine's yaw angle exceeded 10°, the asymmetry of the upper wake profile and the lower wake profile became prominent gradually. This indicates that the degree of wake deflection at different altitudes was different. When the wind turbine was at a relatively large yaw condition, the lower wake profile and the middle wake profile showed a sharp decrease in wake at the far wake. In addition, the asymmetry of the wake profile with respect to the wake center also increased with the increase of the yaw angle. When the yaw angle exceeded 20°, the far wake profile at 0.5 R below the hub height shows a different shape instead of a Gaussian shape. These complex characteristics of a velocity deficit distribution indicate that the evolution mechanism of a yawed wind turbine is complicated. Furthermore, the above analysis may indicate that the Gaussian shape cannot fully describe the complex wake velocity distribution of yawed wind turbines.

3.2. Flow Field Characteristics in the Vertical Section

The complex flow at the horizontal section can be related to the flow on the vertical section to some extent. Figure 7 shows the dimensionless wake velocity contours at different downstream distances. When the wind turbine is not in a yaw condition, regardless of the tower, wind shear, and atmospheric stability, the ideal wind turbine's wake distribution is circular at the vertical cross-section. However, an asymmetrical kidney-shape velocity deficit distribution can be seen in a wake velocity deficit. With an increasing yaw angle, the wake distribution became more distorted. When the wake was fully developed, the upper-height part of the wake was wider than the lower-height part, and the wake of the yawed turbine was much narrower than that of an un-yawed one. When the yaw angle was large and the wake development distance was long, the vertical section of the wake velocity distribution was distorted from the kidney shape to a "hook" shape. In general, in addition to the reduction of the wake velocity deficit area of a yawed wind turbine that was caused by the decrease of the projected area of the wind turbine in the incoming wind direction, the wake of a yawed wind turbine also developed into the well-known kidney shape with the evolution of the wind turbine's wake. Another important wake characteristic is that the center of the wake of a yawed wind turbine moved upward with the development of the wake, and it can be seen that the area with largest velocity deficit was located above hub height. The complex characteristics of the wake of a yawed wind turbine in the vertical section can explain the shape of the horizontal section variation at different heights. Based on the above analysis, if the downstream wind turbine was directly affected by the wake of the upstream wind turbine, the wake impact of the downstream wind turbine was uneven, which brings challenges to the safe and stable operation of wind turbines. The wake deficit in a three-dimensional perspective is shown in Figure 8, and the deflection and deformation of a yawed turbine's wake are also visualized.

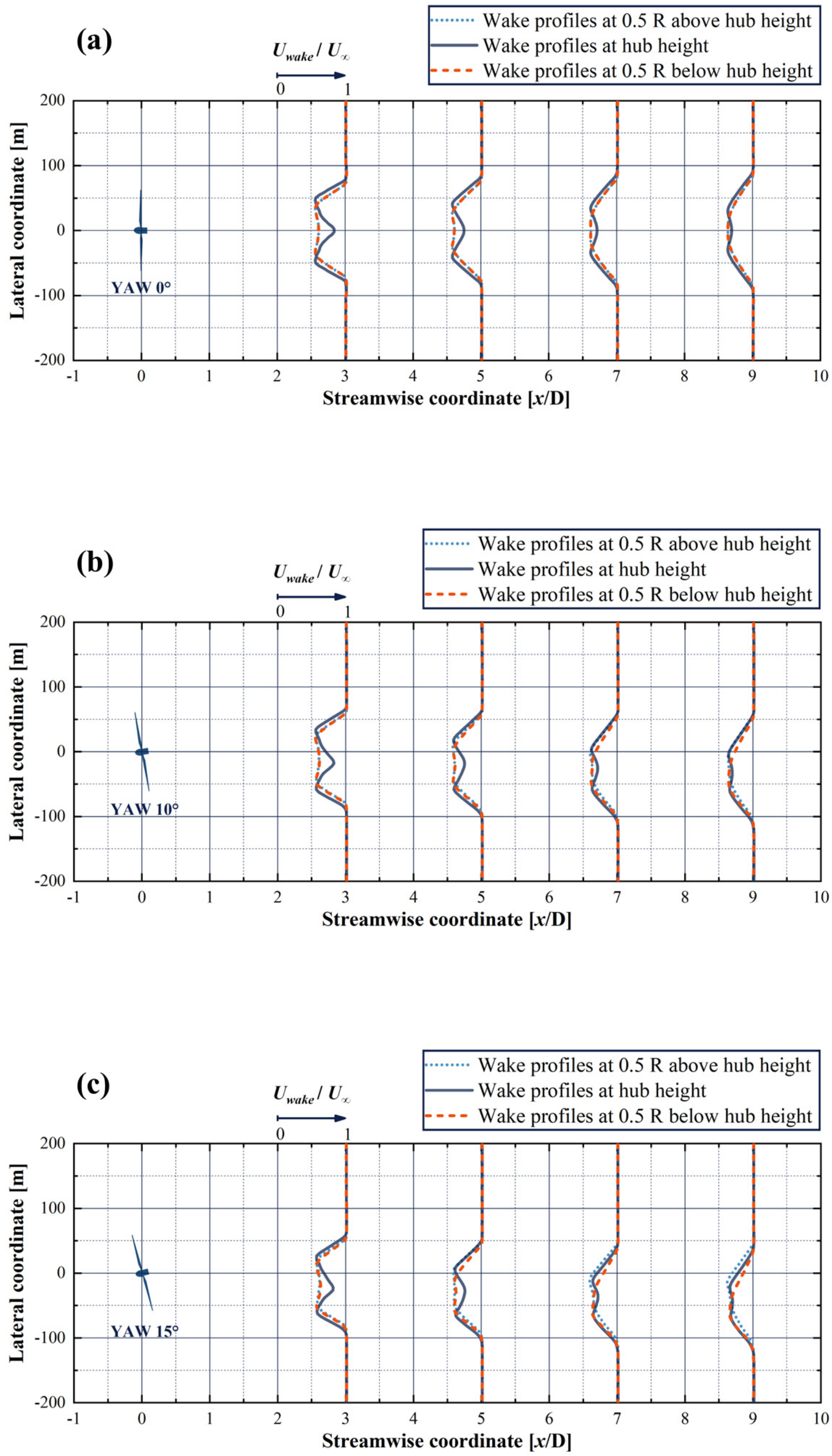

Figure 6. *Cont.*

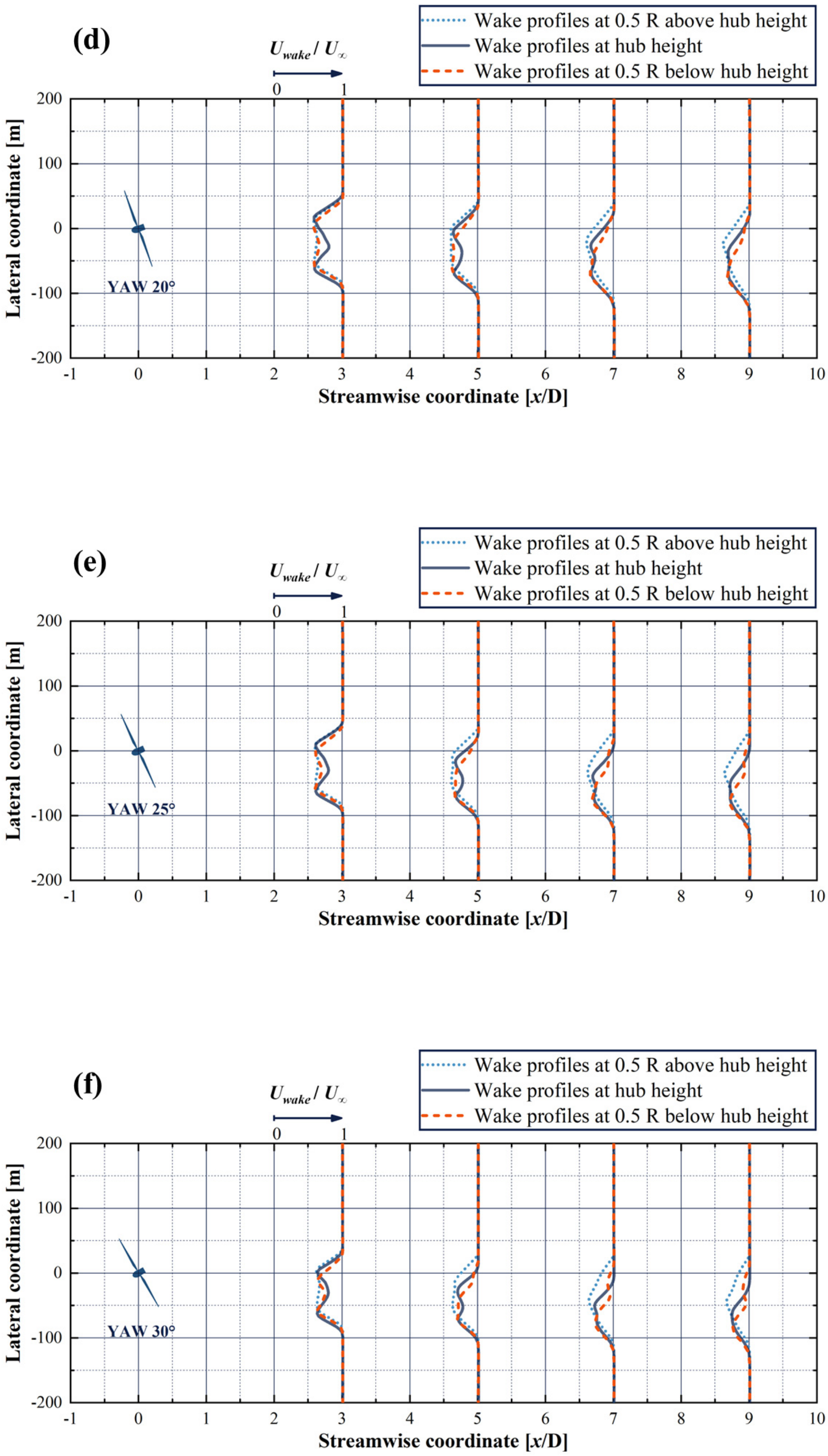

Figure 6. Wake profiles of different yawed wind turbines.

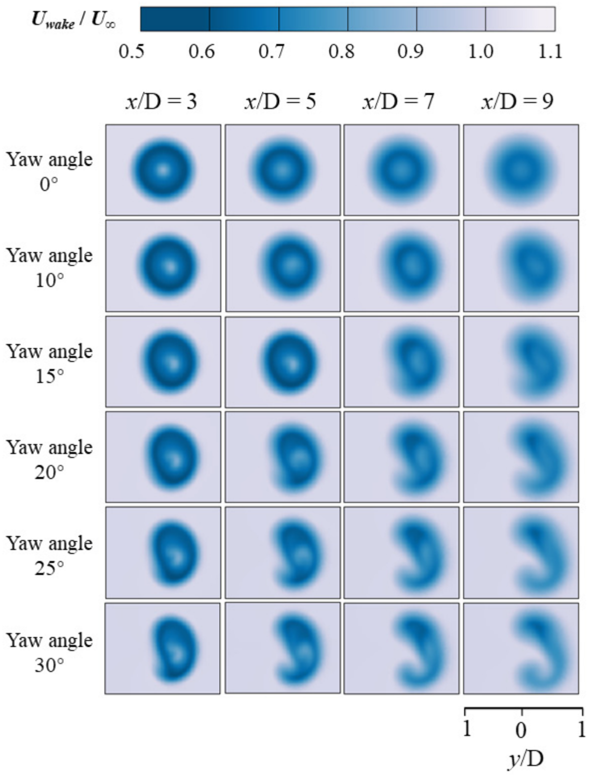

Figure 7. Dimensionless wake velocity contours at different downstream distances.

The direct cause of an asymmetrical kidney-shape distribution is the momentum exchange caused by vorticity in the flow direction. Figure 9 shows the vorticity in the x direction, and the x direction is the incoming wind direction. According to the Biot–Savart law, the vortex in the x direction is directly responsible for the evolution of a velocity deficit distribution in the vertical section, while the induced drag force generated by vorticity in the other two directions is responsible for the wind turbine's thrust force. CVP's formation mechanism is as follows [42]: The velocity circulation on the blade falls off from the blade tip, forming a tip vortex. The periodic rotation of the blade tip leads to the change of velocity circulation shedding, and the velocity circulation in the flow direction carried by the tip vortex is equal to the vortex flux of the CVP.

When the wind turbine was not in yaw conditions, the vortex system consisted of the component of the blade root vortex in the flow direction and the component of the vortex cylinder formed by the tip vortex in the flow direction. The blade root vortex component formed the circular negative vorticity area in the wake's center, while the tip vortex component formed the annular positive vorticity area around the center. With the development of wake, the general distribution of vortex structure hardly changed.

When wind turbine was in yaw conditions, the vortex system was composed of a counter-rotating vortex pair (including the top vortex and bottom vortex) and the blade root vortex. The top vortex and the blade vortex both showed negative vorticity while the bottom vortex showed positive vorticity. The wake structure is shown more intuitively in Figure 10.

Firstly, the vorticity contours of $x/\mathrm{D} = 3$ were analyzed. When yaw angle was 10°, the counter-rotating vortex pair showed a ring distribution, and negative vorticity appeared in the upper left of the wind turbine's wake. This was caused by the periodic change of the blade tip's rotation speed in the flow direction. When the yaw angle kept increasing, the area of negative vorticity gradually increased, and both negative and positive vorticity were much stronger. This was caused by the increase of the blade tip's velocity in the flow direction, which enhanced the vorticity conversion.

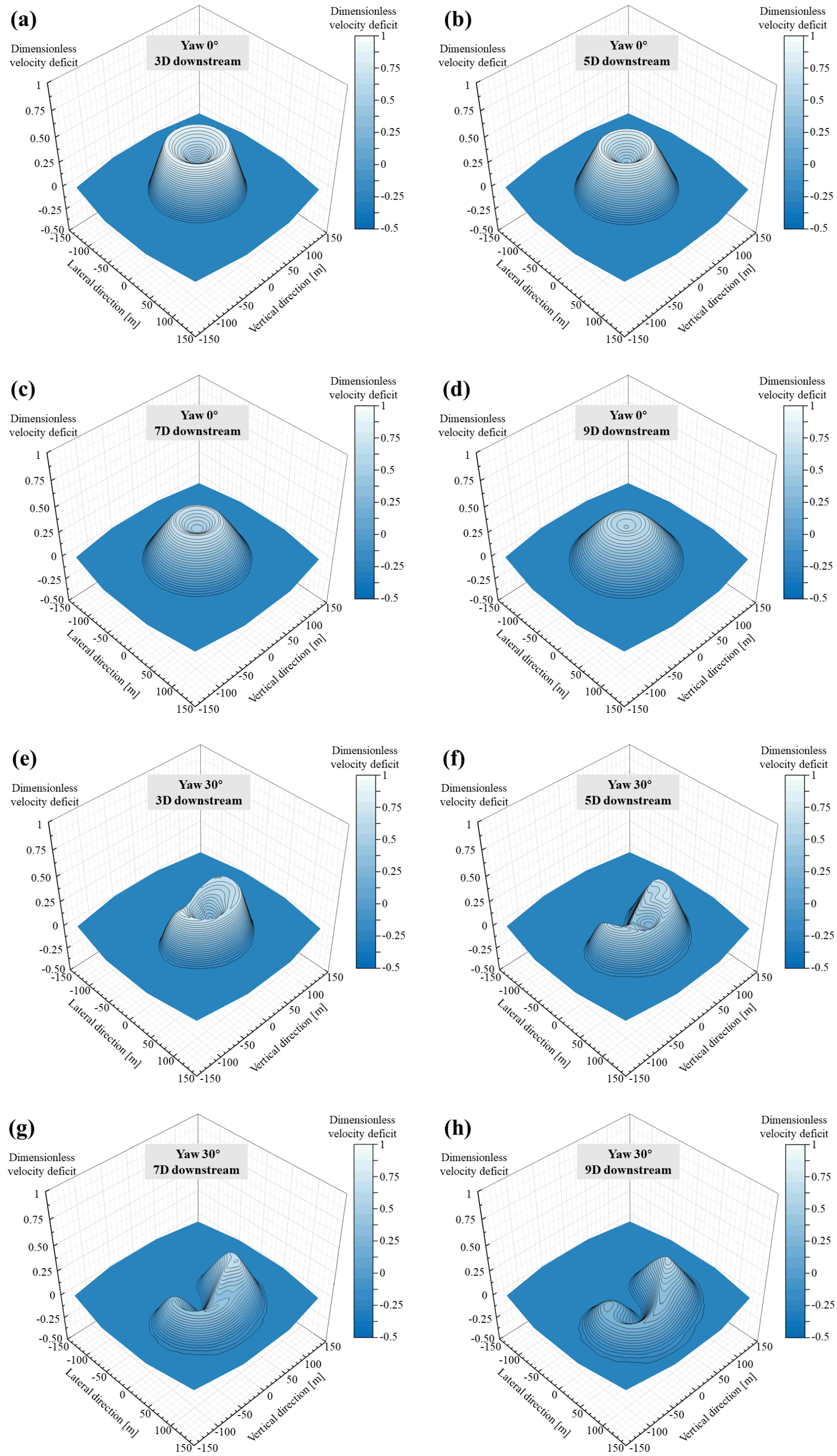

Figure 8. Dimensionless wake velocity contours at different downstream distances in a three-dimensional perspective.

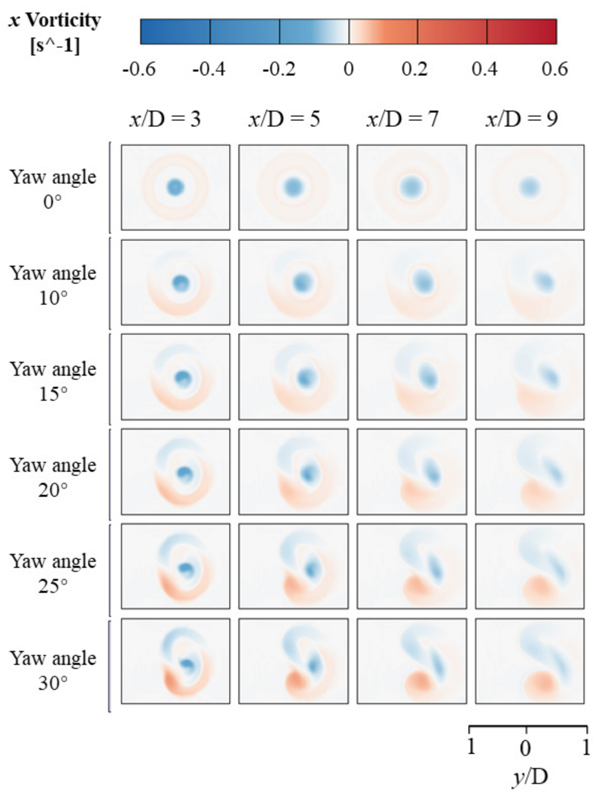

Figure 9. Vorticity contours of the x direction at different downstream distances.

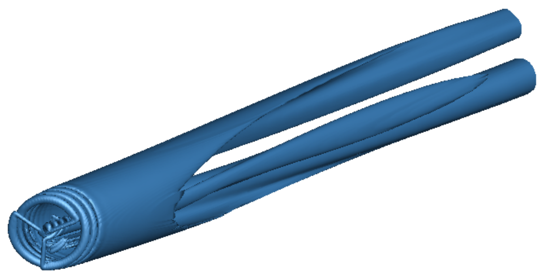

Figure 10. Wake structure of a yawed turbine.

Then, the evolution of the vortex structure of different downstream distances was analyzed. It can be seen that during the development of the wake vortex structure, the blade root vortex tended to break out of CVP. The larger the yaw angle, the more obvious this trend. In addition, under the induction of CVP, the root vortex tended to fuse with the top vortex, which caused the asymmetric deformation of the wake and was the reason for the rise of the wake velocity deficit in Figure 7.

Overall, CVP played a dominating role in the yawed turbine's wake evolution. With the evolution of wind turbine's wake induced by the vorticity field, the vortex structure moved to the right as a whole, with the maximum displacement at about the hub height. Then, a kidney-shape wake structure was formed.

4. Conclusions

Deflection and deformation are the main characteristics of a horizontal wake profile of a yawed wind turbine. In this paper, the velocity deficit shape of a yawed turbine's wake was presented in different ways. It is well known that a yaw wake will deflect, and the deflection can be explained by the conservation of momentum in the lateral direction. However, the asymmetry characteristics could not be interpretated perfectly by this traditional perspective. The turbine's wake deflected to one side that was opposite to the yaw direction, and the increase of the wake deflection below the hub height was much more obvious. The asymmetry of a yawed turbine's wake in the horizontal section was mainly presented in two aspects: the horizontal wake profile at 0.5 R above the hub height (higher profile) and the horizontal wake profile at 0.5 R below the hub height (lower profile) were not basically the same as with the un-yawed one. Another asymmetry was the symmetry of the wake profile itself in the transverse direction. When the turbine was not in a yaw condition, the wake profile showed a symmetrical Gaussian shape. A typical velocity deficit distribution was the far wake profile at 0.5 R below the hub height showing "The Big Dipper" shape instead of a Gaussian shape. This means that the wake had a larger width on the deflected side.

The complex flow at the horizontal section can be related to the flow on the vertical section to some extent. The wake of a yawed wind turbine develops into the well-known kidney shape with the evolution of a wind turbine's wake. This special shape makes possible the complex variation of the wake in the horizontal section. CVP plays a dominating role in a yawed turbine's wake evolution. The induction effect of CVP can be described by the Biot–Savart law. In conclusion, the momentum exchange caused by a yawed turbine's wake vortex structure leads to a complex wake evolution.

Author Contributions: Conceptualization, T.W., C.C. and Q.L.; methodology, T.W., S.Z. and C.C.; software, T.W. and C.C.; formal analysis, K.S., X.W. and Z.W.; investigation, X.Z., S.Z. and Y.Z.; resources, C.C. and Q.L.; writing—original draft preparation, T.W. and C.C.; writing—review and editing, C.C. and Q.L.; visualization, S.Z.; supervision, Q.L.; project administration, Q.L.; funding acquisition, Q.L. All authors have read and agreed to the published version of the manuscript.

Funding: The work was financially supported by the National Key R&D Program of China (No. 2022YFE0207000), the National Natural Science Foundation of China (No. 52176212), the National Engineering Research Center for Offshore Windpower (No. HSFD22001) and the Guangdong Branch of the National Engineering Research Center for Offshore Windpower (No. 2019B090904005).

Informed Consent Statement: Not applicable.

Data Availability Statement: Not applicable.

Conflicts of Interest: The authors declare no conflict of interest.

References

1. Stevens, R.J.; Meneveau, C. Flow Structure and Turbulence in Wind Farms. *Annu. Rev. Fluid Mech.* **2017**, *49*, 311–339. [CrossRef]
2. Gao, X.; Wang, T.; Li, B.; Sun, H.; Yang, H.; Han, Z.; Wang, Y.; Zhao, F. Investigation of wind turbine performance coupling wake and topography effects based on LiDAR measurements and SCADA data. *Appl. Energy* **2019**, *255*, 113816. [CrossRef]
3. Guo, N.-Z.; Shi, K.-Z.; Li, B.; Qi, L.-W.; Wu, H.-H.; Zhang, Z.-L.; Xu, J.-Z. A physics-inspired neural network model for short-term wind power prediction considering wake effects. *Energy* **2022**, *261*, 125208. [CrossRef]
4. Wang, T.; Cai, C.; Wang, X.; Wang, Z.; Chen, Y.; Song, J.; Xu, J.; Zhang, Y.; Li, Q. A new Gaussian analytical wake model validated by wind tunnel experiment and LiDAR field measurements under different turbulent flow. *Energy* **2023**, *271*, 127089. [CrossRef]
5. Yuan, Z.; Sheng, Q.; Sun, K.; Zang, J.; Zhang, X.; Jing, F.; Ji, R. The Array Optimization of Vertical Axis Wind Turbine Based on a New Asymmetric Wake Model. *J. Mar. Sci. Eng.* **2021**, *9*, 820. [CrossRef]
6. Tian, L.; Song, Y.; Xiao, P.; Zhao, N.; Shen, W.; Zhu, C. A new three-dimensional analytical model for wind turbine wake turbulence intensity predictions. *Renew. Energy* **2022**, *189*, 762–776. [CrossRef]
7. Zhang, S.; Gao, X.; Lin, J.; Xu, S.; Zhu, X.; Sun, H.; Yang, H.; Wang, Y.; Lu, H. Discussion on the spatial-temporal inhomogeneity characteristic of horizontal-axis wind turbine's wake and improvement of four typical wake models. *J. Wind. Eng. Ind. Aerodyn.* **2023**, *236*, 105368. [CrossRef]
8. Burton, T.; Jenkins, N.; Sharpe, D.; Bossanyi, E. *Wind Energy Handbook*; John Wiley & Sons: Hoboken, NJ, USA, 2011.
9. Lignarolo, L.E.M.; Ragni, D.; Scarano, F.; Ferreira, C.J.S.; van Bussel, G.J.W. Tip-vortex instability and turbulent mixing in wind-turbine wakes. *J. Fluid Mech.* **2015**, *781*, 467–493. [CrossRef]
10. Du, B.; Ge, M.; Zeng, C.; Cui, G.; Liu, Y. Influence of atmospheric stability on wind-turbine wakes with a certain hub-height turbulence intensity. *Phys. Fluids* **2021**, *33*, 055111. [CrossRef]
11. Elgendi, M.; AlMallahi, M.; Abdelkhalig, A.; Selim, M.Y. A review of wind turbines in complex terrain. *Int. J. Thermofluids* **2023**, *17*, 100289. [CrossRef]
12. Dar, A.S.; Porté-Agel, F. Wind turbine wakes on escarpments: A wind-tunnel study. *Renew. Energy* **2021**, *181*, 1258–1275. [CrossRef]

13. Bastankhah, M.; Porté-Agel, F. Experimental and theoretical study of wind turbine wakes in yawed conditions. *J. Fluid Mech.* **2016**, *806*, 506–541. [CrossRef]
14. Zong, H.; Porté-Agel, F. Experimental investigation and analytical modelling of active yaw control for wind farm power optimization. *Renew. Energy* **2021**, *170*, 1228–1244. [CrossRef]
15. Cheng, S.; Elgendi, M.; Lu, F.; Chamorro, L.P. On the Wind Turbine Wake and Forest Terrain Interaction. *Energies* **2021**, *14*, 7204. [CrossRef]
16. Xiaoxia, G.; Luqing, L.; Shaohai, Z.; Xiaoxun, Z.; Haiying, S.; Hongxing, Y.; Yu, W.; Hao, L. LiDAR-based observation and derivation of large-scale wind turbine's wake expansion model downstream of a hill. *Energy* **2022**, *259*, 125051. [CrossRef]
17. Li, Q.; Maeda, T.; Kamada, Y.; Mori, N. Investigation of wake effects on a Horizontal Axis Wind Turbine in field experiments (Part I: Horizontal axis direction). *Energy* **2017**, *134*, 482–492. [CrossRef]
18. Sørensen, J.N.; Shen, W.Z. Numerical Modeling of Wind Turbine Wakes. *J. Fluids Eng.* **2002**, *124*, 393–399. [CrossRef]
19. Martín-San-Román, R.; Benito-Cia, P.; Azcona-Armendáriz, J.; Cuerva-Tejero, A. Validation of a free vortex filament wake module for the integrated simulation of multi-rotor wind turbines. *Renew. Energy* **2021**, *179*, 1706–1718. [CrossRef]
20. Chen, Z.; Wang, X.; Guo, Y.; Kang, S. Numerical analysis of unsteady aerodynamic performance of floating offshore wind turbine under platform surge and pitch motions. *Renew. Energy* **2020**, *163*, 1849–1870. [CrossRef]
21. Jensen, N.O. *A Note on Wind Generator Interaction*; Risø National Laboratory: Roskilde, Denmark, 1983.
22. Bastankhah, M.; Porté-Agel, F. A new analytical model for wind-turbine wakes. *Renew. Energy* **2014**, *70*, 116–123. [CrossRef]
23. Du, B.; Ge, M.; Liu, Y. A physical wind-turbine wake growth model under different stratified atmospheric conditions. *Wind. Energy* **2022**, *25*, 1812–1836. [CrossRef]
24. Tian, L.; Zhu, W.; Shen, W.; Zhao, N.; Shen, Z. Development and validation of a new two-dimensional wake model for wind turbine wakes. *J. Wind. Eng. Ind. Aerodyn.* **2015**, *137*, 90–99. [CrossRef]
25. Chiang, Y.-C.; Hsu, Y.-C.; Chau, S.-W. Power Prediction of Wind Farms via a Simplified Actuator Disk Model. *J. Mar. Sci. Eng.* **2020**, *8*, 610. [CrossRef]
26. Barthelmie, R.J.; Hansen, K.; Frandsen, S.T.; Rathmann, O.; Schepers, J.G.; Schlez, W.; Phillips, J.; Rados, K.; Zervos, K.; Politis, E.S.; et al. Modelling and Measuring Flow and Wind Turbine Wakes in Large Wind Farms Offshore. *Wind. Energy* **2009**, *12*, 431–444. [CrossRef]
27. Barthelmie, R.J.; Pryor, S.C.; Frandsen, S.T.; Hansen, K.S.; Schepers, J.G.; Rados, K.; Schlez, W.; Neubert, A.; Jensen, L.E.; Neckelmann, S. Quantifying the Impact of Wind Turbine Wakes on Power Output at Offshore Wind Farms. *J. Atmospheric Ocean. Technol.* **2010**, *27*, 1302–1317. [CrossRef]
28. Barthelmie, R.J.; Jensen, L.E. Evaluation of wind farm efficiency and wind turbine wakes at the Nysted offshore wind farm. *Wind. Energy* **2010**, *13*, 573–586. [CrossRef]
29. Wei, D.; Wang, N.; Wan, D.; Strijhak, S. Parametric study of the effectiveness of active yaw control based on large eddy simulation. *Ocean Eng.* **2023**, *271*, 113751. [CrossRef]
30. Yang, S.; Deng, X.; Ti, Z.; Yan, B.; Yang, Q. Cooperative yaw control of wind farm using a double-layer machine learning framework. *Renew. Energy* **2022**, *193*, 519–537. [CrossRef]
31. Nakhchi, M.; Naung, S.W.; Rahmati, M. A novel hybrid control strategy of wind turbine wakes in tandem configuration to improve power production. *Energy Convers. Manag.* **2022**, *260*, 115575. [CrossRef]
32. Dou, B.; Qu, T.; Lei, L.; Zeng, P. Optimization of wind turbine yaw angles in a wind farm using a three-dimensional yawed wake model. *Energy* **2020**, *209*, 118415. [CrossRef]
33. Song, J.; Kim, T.; You, D. Particle swarm optimization of a wind farm layout with active control of turbine yaws. *Renew. Energy* **2023**, *206*, 738–747. [CrossRef]
34. Ma, H.; Ge, M.; Wu, G.; Du, B.; Liu, Y. Formulas of the optimized yaw angles for cooperative control of wind farms with aligned turbines to maximize the power production. *Appl. Energy* **2021**, *303*, 117691. [CrossRef]
35. Li, B.; He, J.; Ge, M.; Ma, H.; Du, B.; Yang, H.; Liu, Y. Study of three wake control strategies for power maximization of offshore wind farms with different layouts. *Energy Convers. Manag.* **2022**, *268*, 116059. [CrossRef]
36. Dou, B.; Guala, M.; Lei, L.; Zeng, P. Wake model for horizontal-axis wind and hydrokinetic turbines in yawed conditions. *Appl. Energy* **2019**, *242*, 1383–1395. [CrossRef]
37. Zhu, X.; Chen, Y.; Xu, S.; Zhang, S.; Gao, X.; Sun, H.; Wang, Y.; Zhao, F.; Lv, T. Three-dimensional non-uniform full wake characteristics for yawed wind turbine with LiDAR-based experimental verification. *Energy* **2023**, *270*, 126907. [CrossRef]
38. Jiménez, Á.; Crespo, A.; Migoya, E. Application of a LES technique to characterize the wake deflection of a wind turbine in yaw. *Wind. Energy* **2009**, *13*, 559–572. [CrossRef]
39. Micallef, D.; van Bussel, G.; Ferreira, C.S.; Sant, T. An investigation of radial velocities for a horizontal axis wind turbine in axial and yawed flows. *Wind. Energy* **2013**, *16*, 529–544. [CrossRef]
40. Howland, M.F.; Bossuyt, J.; Martínez-Tossas, L.A.; Meyers, J.; Meneveau, C. Wake structure in actuator disk models of wind turbines in yaw under uniform inflow conditions. *J. Renew. Sustain. Energy* **2016**, *8*, 043301. [CrossRef]
41. Shapiro, C.R.; Gayme, D.F.; Meneveau, C. Modelling yawed wind turbine wakes: A lifting line approach. *J. Fluid Mech.* **2018**, *841*, 12. [CrossRef]

42. Wang, T.; Cai, C.; Wang, X.; Wang, Z.; Chen, Y.; Hou, C.; Zhou, S.; Xu, J.; Zhang, Y.; Li, Q. Evolution mechanism of wind turbine wake structure in yawed condition by actuator line method and theoretical analysis. *Energy Convers. Manag.* **2023**, *281*, 116852. [CrossRef]
43. Abdelkhalig, A.; Elgendi, M.; Selim, M.Y. Review on validation techniques of blade element momentum method implemented in wind turbines. *IOP Conf. Ser. Earth Environ. Sci.* **2022**, *1074*, 012008. [CrossRef]
44. Jonkman, J.; Butterfield, S.; Musial, W.; Scott, G. *Definition of a 5MW Reference Wind Turbine for Offshore System Development*; National Renewable Energy Lab (NREL): Golden, CO, USA, 2009.